Observation of a resonant structure in the cross section of $e^+e^- \to \phi\ \eta'$ at center-of-mass energies between 2.050 and 3.080 GeV

(Dated: March 13, 2019)

Based on data samples collected with the BESIII detector at the BEPCII collider at 22 center of mass energies from 2.0 to 3.08 GeV, we search for the production of $e^+e^- \to \phi\ \eta'$. The Born cross sections of $e^+e^- \to \phi\ \eta'$ process are observed for the first time. Assuming the $\phi\ \eta'$ signals from a single resonance, we extract the mass and width of the resonance to be (2182.4 ± 5.1 ± 1.6) MeV/c^2 and (142.2 ± 16.6 ± 0.0) MeV, respectively, and the statistical significance is more than 12σ.

PACS numbers: 13.25.Gv, 12.38.Qk, 14.20.Gk, 14.40.Cs

I. INTRODUCTION

The $\phi(2170)$ resonance was first discovered in the process $e^+e^- \to \phi f_0(980)$ by the BABAR [1] via initial-state radiation (ISR) technique and then confirmed by Belle [2]. BES [3] and BESIII [4, 5] also observed the $\phi(2170)$ in the $\phi f_0(980)$ invariant mass spectrum. The state does not fit into the conventional strangenium spectrum of the quark model. In addition, even though the mass of the $\phi(2170)$ is well above the $K\bar{K}$ threshold, it has not yet been found to decay to $K\bar{K}$ [6], in contrast to the conventional strangenium states in this mass region.

There are several theoretical interpretations of $\phi(2170)$, including a $s\bar{s}g$ hybrid [7, 8], a 2^3D_1 [9] or 3^3S_1 $s\bar{s}$ [10], a tetraquark state [11, 12], a $\Lambda\bar{\Lambda}$ bound state [13, 14], an S-wave threshold effects [15], or a three-meson system ϕK^+K^- [16]. The $3^3S_1 s\bar{s}$ state is predicted to have significant branching fractions to the $s\bar{s}$-signature modes $\phi\eta$ and $\phi\eta'$, whereas the decay couplings of any $n\bar{n}$ (where n≡u, d) state to anything + ϕ should be weak. Although the $\phi\eta'$ mode of the hybird should be weak, the $s\bar{s}$-hybrid vector should also have a large $\phi\eta$ branching fraction [10]. The different decay modes of 2^3D_1 $s\bar{s}$ state had been studied [9]. There are significant difference between two modes' width. The $\phi\eta$ mode should be useful in establishing the true mass and width of the $3^3S_1 s\bar{s}$ state, since interference with nonstrange vectors should be unimportant in this channel. The prediction of a branching fraction ratio of $B_{\phi(2170)\to\phi\eta/\phi\eta'}$ should be reliable, as shown in the Table I. $\phi(2170)$ dominantly decays into $\phi\eta$ and $\phi\eta'$ in the tetraquark picture under the assumption that the tetraquark prefers to rearrange into two mesons, so the processes of $e^+e^- \to \eta\phi$ and $e^+e^- \to \eta'\phi$ also provides a good opportunity to study strangeonium vector states above the $K\bar{K}$ production threshold.

BABAR Collaboration has measured the cross section of $e^+e^- \to \gamma\phi\eta$ via the initial-state radiation process and observed a structure at 2.13 GeV [18]. In a study of ISR events of the type, $e^+e^- \to \gamma_{ISR}\eta'\phi$, the BABAR Collaboration observed several signal events [19]. Because of the low statistics for $e^+e^- \to \gamma_{ISR}\eta'\phi$, they did not carry out further study. BESIII has studied of $J/\psi \to \phi\eta\eta'$ decay and reported the observation of the structure at 2.002 GeV/c^2 by assuming the J^P value of the structure as 1^- [17]. Experimental study of $e^+e^- \to \phi\ \eta'$ with large data samples in this energy region may shed light on the nature of the $\phi(2170)$ state.

The analysis is based on a data sample of 650 pb^{-1} collected at the Beijing spectrometer (BESIII) with center-of-mass energies (c.m. energies) ranging from 2.0 to 3.08 GeV to measure the Born cross sections of the reactions $e^+e^- \to \phi\ \eta'$. To identify whether or nor the $\phi\ \eta'$ system originates from a $\phi(2170)$, the energy dependence of the $e^+e^- \to \phi\ \eta'$ cross section is compared to that of $\phi f_0(980)$.

TABLE I: The partial decay width of $Y(2175)$ decay as 2^3D_1 and $3^3S_1 s\bar{s}$ and $1^{--} s\bar{s}g$ in the $^3P_0$ model and flux tube model.

Decay Modes	1^{--} $s\bar{s}g$ [7]	$2^3D_1 s\bar{s}$ [9]		$3^3S_1 s\bar{s}$ [10]
	Flux tube	$^3P_0$ model	flux tube	$^3P_0$ model
$\phi\ \eta$	1.2	0	0	21
$\phi\ \eta'$	0.4	2.9	2.8	11
$B_{\phi\eta/\phi\eta'}$	3	0	0	1.9

II. DETECTOR AND DATA SAMPLES

The BESIII detector is a magnetic spectrometer [20] located at the Beijing Electron Position Collider (BEPCII) [21]. The cylindrical core of the BESIII detector consists of a helium-based multilayer drift chamber (MDC), a plastic scintillator time-of-flight system (TOF), and a CsI(Tl) electromagnetic calorimeter (EMC), which are all enclosed in a superconducting solenoidal magnet providing a 1.0 T magnetic field. The solenoid is supported by an octagonal flux-return yoke with resistive plate counter muon identifier modules interleaved with steel. The acceptance of charged particles and photons is 93% over 4π solid angle. The charged-particle momentum resolution at 1 GeV/c is 0.5%, and the dE/dx resolution is 6% for the electrons from Bhabha scattering. The EMC measures photon energies with a resolution of 2.5% (5%) at 1 GeV in the barrel (end cap) region. The time resolution of the TOF barrel part is 68 ps, while that of the end cap part is 110 ps.

The optimization of selection criteria, the determination of detection efficiencies and estimations of potential backgrounds are performed based on Monte Carlo (MC) simulations taking the various aspects of the experimental setup into account. A GEANT4-based [22] MC simulation software, which includes geometric and material description of the BESIII detector, the detector response and digitisation models, as well as accounting of the detector running conditions and performances, is used to generate the MC samples.

For the background study, the process of $e^+e^- \to q\bar{q}$ is simulated by the MC event generator CONEXC [23], while the decays are generated by EVTGEN [24, 25] for known decay modes with branching fractions set to Particle Data Group (PDG) world average values [26] and by LUARLW [27] for the remaining unknown decays. The signal MC samples from $e^+e^- \to \phi\eta'$ is generated at c.m. energies corresponding to the experimental values, where the line shape of the production cross section of the process is taken from the BABAR experiment [18].

III. EVENT SELECTION

For the process $e^+e^- \to \phi\ \eta'$, the ϕ candidate is reconstructed with K^+K^- and the η' is via $\pi^+\pi^-\gamma$ decay mode. Candidate events are required to have three or four charged tracks and at least one photon candidates.

- Good charged tracks: Charged tracks are reconstructed from hits in the MDC within the polar angle range $|\cos\theta| < 0.93$. The tracks are required to pass the interaction point within 10 cm along the beam direction and within 1 cm in the plane perpendicular to the beam.

- Particle identification: For each charged track, the TOF and the dE/dx information combined to form particle identification confidence levels (C.L.) for the π, K, and p hypotheses, and the particle type with the highest C.L. is assigned to each track. At least one kaon is required to be identified.

- Good photon: Photon candidate is reconstructed from isolated showers in the EMC, and the corresponding energies are required to be at least 25 MeV in the barrel ($|\cos\theta| < 0.80$) or 50 MeV in the end caps ($0.86 < |\cos\theta| < 0.92$). To eliminate showers associated with charged particles, the angle between the cluster and the nearest charged track must be larger than 10 degrees. An EMC cluster timing requirement of $0 < t < 700$ ns is also applied to suppress electronic noise and energy deposits unrelated to the event.

- Vertex fit : The primary vertex of the event is reconstructed by two pions and one kaon.

- One-constraint (1C) kinematic fit : 1C kinematic fit is performed under the hypothesis that the $K\pi^+\pi^-\gamma$ missing mass corresponds to the kaon mass. For events with two reconstructed and identified kaons, the combination with the smallest chi-square of 1C kinematic fit is retained. The corresponding χ^2, denoted as $\chi^2_{1C}(\pi^+\pi^-KK_{miss}\gamma)$, is required to be less than 20.

- Mass window of ϕ: The candidate event is required to be within the ϕ signal region, defined as $|\ M(K^+K^-) - M_\phi\ | < 0.015$ GeV.

- Energy of photon : In order to suppress the background processes, the energy of photons is required to be larger than 70 MeV.

After applying the above selection criteria, the momentum distributions are shown in Fig. 1, where the M(K^+K^-) is required to be in the ϕ mass range, $|M(K^+K^-) - m_\phi| < 0.01 GeV/c^2$, and m_ϕ is the nominal ϕ mass from PDG [26].

IV. SIGNAL YIELDS

The signal yields of $e^+e^- \to \phi\ \eta'$ are observed from unbinned maximum likelihood fits to the $\pi^+\pi^-\gamma$ invariant-mass spectrum. The signal is described by the line shape obtained from the MC simulation convoluted with a Gaussian function, which account for the difference in resolution between data and MC simulation. The background shape is parametrized by a second-order polynomial function. The parameters of the Gaussian function and the polynomial function are left free in the fit. The corresponding fit result is shown in Fig. 2 at $\sqrt{s} = 2.125$ GeV.

The same event selection criteria and fit procedure are implemented on the other 19 data samples taken at different c.m. energies. The number of events for these samples are listed in Table II.

V. EXTRACTION OF THE BORN CROSS SECTION

The Born cross section is calculated by:

$$\sigma^B = \frac{N^{obs}}{\mathcal{L}\cdot(1+\delta)\cdot\epsilon\cdot\mathcal{B}}, \tag{1}$$

where N^{obs} is the number of observed signal events, $\mathcal{L}$ is the integrated luminosity, $(1+\delta)$ stands for $(1+\delta^{\mathrm{r}})\cdot(1+\delta^{\mathrm{v}})$, $(1+\delta^{\mathrm{r}})$ is initial state radiation (ISR) correction

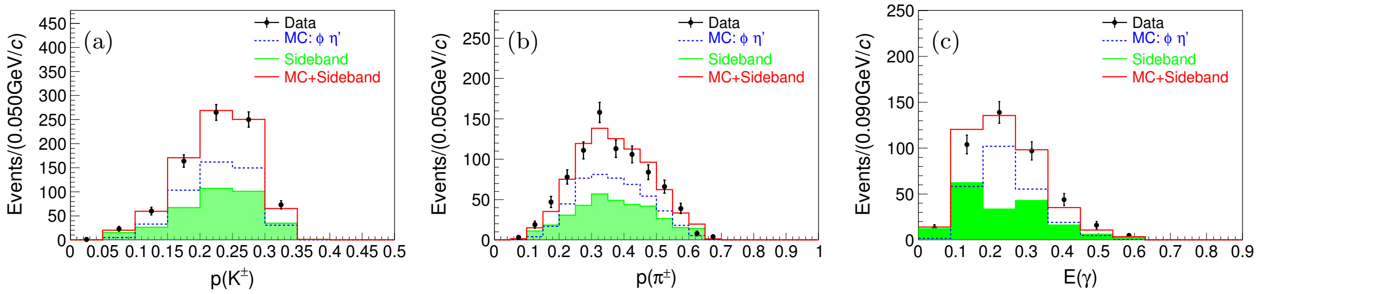

FIG. 1: The momentum spectrum of $K^{\pm}$ (a) and $\pi^{\pm}$ (b), the energy spectrum of γ (c). The black dots with error bars are data, the hatched (green) histogram is the background from ϕ sideband region, the dashed histogram is $\phi\eta'$ MC, the solid (red) histogram is the sum of MC and the background.

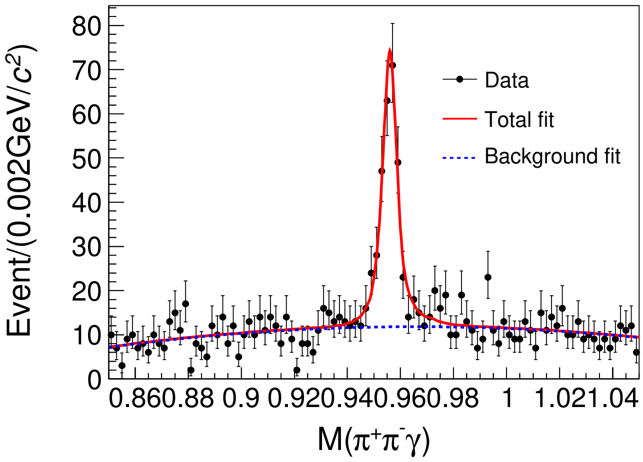

FIG. 2: (color online). The fit to the M($\pi^+\pi^-\gamma$) mass spectrum at $\sqrt{s}$=2.125 GeV. The black dots with error bars are for data, the solid (red) curve for the total fit result and the dashed (blue) curve for the background from the fit.

factor, which is obtained by QED calculation [28] and taking the line shape of the Born cross section measured by the BABAR experiment. The vacuum polarization factor $(1+\delta^{\rm v})$ is taken from QED calculation with an accuracy of 0.5% [29], ϵ is the detection efficiency including reconstruction and all selection criteria, $\mathcal{B}$ is the product branching ratio and $\mathcal{B}(\phi \to K^+K^-)\cdot\mathcal{B}(\eta' \to \pi^+\pi^-\gamma)$, taken from the Particle Data Group (PDG) [26].

Both ϵ and $(1+\delta)$ are obtained from MC simulations of the signal reaction at the individual c.m. energies. In the CONEXC generator, the cross section for the ISR process ($\sigma_{e^+e^-\to\gamma X}$) is parameterized using

$$\sigma_{e^+e^-\to\gamma X} = \int d\sqrt{s'}\frac{2\sqrt{s'}}{s}W(s,x)\frac{\sigma^B(\sqrt{s'})}{[1-\Pi(\sqrt{s'})]^2}, \quad (2)$$

where $\sqrt{s'}$ is the effective c.m. energy of the final state with $s' = s(1-x)$, x depends on the energy of the radiated photon according to $x = 2E_\gamma/\sqrt{s}$, $W(s,x)$ is the radiator function and $\Pi(\sqrt{s'})$ describes the VP effect. The latter includes contributions from leptons and quarks. The detection efficiency and the radiative correction factor depend on the input cross section, and can only be extracted by an iterative procedure, in which the line shape of the cross section from BABAR is used as the initial, and the updated Born cross section is obtained according to the simulation. We repeat the procedure until the measured Born cross section does not change by more than 0.5%.

The measured Born cross section for $e^+e^- \to \phi\ \eta'$ at each energy point is listed in the Table II.

TABLE II: The Born cross sections of $e^+e^- \to \phi\ \eta'$. The center-of-mass energy ($\sqrt{s}$), integrated luminosity ($\mathcal{L}$), the yields of signal events (N^{obs}), the product of radiative correction factor and vacuum polarization factor $(1+\delta)$, detection efficiency (ϵ), Born cross section (σ^B). The first uncertainties are statistical and the second systematic.

$\sqrt{s}$ (GeV)	$\mathcal{L}$ (pb^{-1})	N^{obs}	$(1+\delta)$	ϵ	σ^B (pb)
2.050	3.34	4.3±3.0	0.8878	0.2569	39.6±27.7±4.3
2.100	12.17	21.3±6.3	0.9258	0.2899	45.8±13.6±3.8
2.125	108.49	267.7±22.2	0.9382	0.2995	61.7±5.1±3.9
2.150	2.84	12.3±4.2	0.9483	0.3098	103.6±35.4±6.9
2.175	10.62	87.4±11.0	0.9567	0.3243	186.3±23.4±11.6
2.200	13.70	105.5±11.8	0.9640	0.3269	171.7±19.2±10.1
2.232	11.86	73.6±10.2	0.9720	0.3313	135.5±18.8±11.8
2.309	21.09	65.6±9.8	0.9772	0.3386	66.1±9.9±4.3
2.386	22.55	52.7±8.8	0.9923	0.3408	48.6±8.1±3.8
2.396	66.87	163.9±15.0	0.9939	0.3428	50.6±4.6±3.0
2.500	1.10	3.7±2.1	1.0069	0.3471	67.8±38.5±4.5
2.644	33.72	73.9±9.5	1.0091	0.3476	43.9±5.6±2.4
2.646	34.00	50.4±8.0	1.0093	0.3462	29.8±4.7±1.8
2.800	1.01	2.0±1.4	0.9964	0.3517	39.8±27.9±2.4
2.900	105.25	113.3±12.0	1.0110	0.3463	21.6±2.3±1.3
2.950	15.94	9.9±3.4	1.0130	0.3425	12.6±4.3±0.8
2.981	16.07	6.9±2.9	1.0124	0.3429	8.7±3.7±0.9
3.000	15.88	12.6±3.7	1.0109	0.3415	16.2±4.7±1.2
3.020	17.29	14.5±4.1	1.0080	0.3400	17.2±4.9±1.2
3.080	126.19	90.2±10.3	0.9056	0.3385	16.4±1.9±1.0

TABLE III: Systematic uncertainties (%) in the cross section of $e^+e^- \to \phi\ \eta'$. They are associated with the luminosity ($\mathcal{L}$), tracking efficiency (Tracking), photon efficiency (Photon), PID efficiency (PID), kinematic fit (Kinematic), signal and background shape (Sig. shape and Bck. shape), fit range (Range), the initial state radiation factor (ISR), the vacuum polarization correction factor (VP), mass window (ϕ Cut), energy of γ (γ Cut), MC statistics (MC), branching fraction ($\mathcal{B}$). The total uncertainty is obtained by summing the individual contributions in quadrature.

$\sqrt{s}$ (GeV)	$\mathcal{L}$	Tracking	Photon	PID	Kinematic	Sig. shape	Bck. shape	Range	ISR	ϕ Cut	γ Cut	MC	$\mathcal{B}$	Sum
2.050	1.0	3.0	1.0	3.0	3.0	0.0	0.0	8.9	0.1	0.6	2.5	0.5	2.0	10.9
2.100	1.0	3.0	1.0	3.0	2.7	0.0	0.9	5.7	0.9	0.6	1.2	0.5	2.0	8.2
2.125	1.0	3.0	1.0	3.0	2.6	0.3	0.4	1.5	0.8	0.6	2.2	0.5	2.0	6.3
2.150	1.0	3.0	1.0	3.0	2.3	0.0	0.8	1.2	0.8	1.1	3.4	0.5	2.0	6.7
2.175	1.0	3.0	1.0	3.0	2.0	1.5	0.7	2.1	1.0	1.1	0.7	0.5	2.0	6.2
2.200	1.0	3.0	1.0	3.0	2.3	0.8	1.6	1.3	0.7	0.1	0.4	0.5	2.0	5.9
2.232	1.0	3.0	1.0	3.0	2.4	1.9	1.5	1.1	0.1	6.2	0.6	0.4	2.0	8.7
2.309	1.0	3.0	1.0	3.0	1.9	2.0	2.9	0.6	0.2	0.6	1.2	0.4	2.0	6.5
2.386	1.0	3.0	1.0	3.0	1.9	2.5	4.7	1.4	0.3	0.5	1.4	0.4	2.0	7.8
2.396	1.0	3.0	1.0	3.0	1.6	0.1	2.0	0.9	0.6	1.6	1.0	0.4	2.0	6.0
2.500	1.0	3.0	1.0	3.0	1.6	0.0	2.7	2.4	0.9	2.0	0.4	0.4	2.0	6.7
2.644	1.0	3.0	1.0	3.0	0.8	0.0	0.8	0.9	0.0	2.0	0.7	0.4	2.0	5.5
2.646	1.0	3.0	1.0	3.0	0.8	0.0	1.4	1.6	0.2	1.8	1.7	0.4	2.0	6.0
2.800	1.0	3.0	1.0	3.0	0.5	0.0	0.0	0.2	0.4	3.5	0.6	0.4	2.0	6.1
2.900	1.0	3.0	1.0	3.0	0.3	1.3	0.3	1.6	0.1	3.2	0.1	0.4	2.0	6.2
2.950	1.0	3.0	1.0	3.0	0.1	1.0	0.0	2.9	0.3	0.7	1.6	0.4	2.0	6.1
2.981	1.0	3.0	1.0	3.0	0.0	0.0	0.0	5.6	0.2	7.7	2.0	0.4	2.0	10.9
3.000	1.0	3.0	1.0	3.0	0.1	0.0	0.8	0.6	0.6	5.1	0.7	0.4	2.0	7.2
3.020	1.0	3.0	1.0	3.0	0.0	0.7	2.1	0.5	0.2	4.2	0.0	0.4	2.0	6.8
3.080	1.0	3.0	1.0	3.0	0.1	0.9	2.0	1.7	1.0	0.6	0.3	0.4	2.0	5.8

VI. SYSTEMATIC UNCERTAINTY

Several sources of systematic uncertainties are considered in the measurement of the Born cross sections. These include luminosity measurements, the differences between the data and the MC simulation for the tracking efficiency, photon's efficiency, PID efficiency, kinematic fit, the fit procedure, mass window requirement of ϕ, energy region of γ, the MC simulation of the ISR correction factor and the vacuum polarization factor, as well as uncertainties in the branching fractions of intermediate state decays and in the luminosity measurements.

(a) *Luminosity:* The integrated luminosity of the data samples used in this analysis are measured using large angle Bhabha events, and the corresponding uncertainties are estimated to be 1.0% [30].

(b) *Tracking:* The uncertainty of the tracking efficiency is investigated using a control sample of $e^+e^- \to K^+K^-\pi^+\pi^-$ process [6]. The difference in tracking efficiency between the data and the MC simulation is estimated to be 1% per track. Hence, 3.0% is taken as the systematic uncertainty for the three selected kaons.

(c) *Photon:* The uncertainty due to photon detection is 1% per photon [31].

(d) *PID:* To estimate the PID efficiency uncertainty, we study $K^\pm$ and $\pi^\pm$ PID efficiencies with the same control samples as those used in the tracking efficiency. The average PID efficiency difference between the data and the MC simulation is found to be 1% per charged track and taken as a systematic uncertainty. Therefore, 3.0% is taken as the systematic uncertainty for the three selected kaons.

(e) *Kinematic fit:* Uncertainty associated with kinematic fits come from the inconsistency of the track helix parameters between the data and the MC simulation. The helix parameters for the charged tracks of MC samples are corrected to eliminate the inconsistency, as described in Ref. [32], and the agreement of χ^2 distributions between the data and the MC simulation is much improved. We take he differences on the selection efficiencies with and without the correction as the systematic uncertainties.

(f) *Mass window of ϕ:* A mass window requirement on the K^+K^- invariant-mass introduces a systematic uncertainty on the efficiency. The difference between $|M(K^+K^-) - M(\phi)| \leq 0.015$ GeV and $|M(K^+K^-) - M(\phi)| \leq 0.020$ GeV is worked as uncertainty.

(g) *Energy of γ:* The difference in the efficiency between $E(\gamma) > 0.07$ GeV and $E(\gamma) > 0.06$ GeV is worked as uncertainty.

(h) *Fitting procedure:* Fit to the invariant-mass of $\pi^+\pi^-\gamma$ to extract the signal yields of $e^+e^- \to \phi\ \eta'$ process. The following three aspects are considered when evaluating the systematic uncertainty associated with the fit procedure.

(1) *Fitting range:* In the fit, the $M(\pi^+\pi^-\gamma)$ is fitted by varying the fitting range from (0.85, 1.05) GeV/c^2 to (0.8, 1.10) GeV/c^2. The difference in the yield are

treated as the systematic uncertainty from the fit range.

(2) *Signal shape:* In the fit, the signal shape is described by a shape obtained from a MC simulation convoluted with a Gaussian function. The uncertainty related to the signal line shape is estimated with an alternative fit using the same function for signal line-shape, but fixing width of Gaussian function to the value by changing one standard deviation of width obtained in the nominal fit. The difference of the yields between them is considered as the systematic uncertainty from the signal shape.

(3) *Background shape:* In the fit, the background shape is described as a second-order polynomial function. The fit with a third-order polynomial function for the background shape is used to estimate its uncertainty.

(i) *ISR factor:* The cross section is measured by iterating until $(1+\delta^r)\times\epsilon$ converges, and the difference between the last two iterations is taken as the systematic uncertainty associated with the ISR correction factor.

(j) *Branching fraction:* The uncertainties in the branching fractions for the processes $\phi \to K^+K^-$ and $\eta' \to \pi^+\pi^-\gamma$ are taken from the PDG [26].

(k) *MC:* The uncertainty is estimated by the number of the generated events.

Assuming all of the above systematic uncertainties, shown in Table III, are independent, the total systematic uncertainties are obtained by adding the individual uncertainties in quadrature.

VII. RESONANCE IN THE LINE SHAPE OF CROSS SECTION OF $e^+e^- \to \phi\ \eta'$

Figure 3 shows the measured Born cross section for $e^+e^- \to \phi\ \eta'$ over the energy region studied in this work. There is a clear structure around 2.200 GeV. To study the possible resonant structure in the $e^+e^- \to \phi\ \eta'$ process, a χ^2 fit incorporating the correlated and uncorrelated uncertainties is performed to the measured cross section. Assuming that the $\phi\ \eta'$ signals come from a resonance decay, we fit the line shape using a coherent sum of a phase-space modified Breit-Wigner (BW) function with a mass-dependent width and a phase-space term. The probability density function (PDF) is parameterized as

$$\mid A(\sqrt{s})\mid^2 = \mid C_0\sqrt{\Phi(\sqrt{s})} + e^{i\varphi}\times BW(\sqrt{s})\mid^2, \quad (3)$$

$$BW(\sqrt{s}) = \frac{M_R}{\sqrt{s}}\frac{\sqrt{12\pi\Gamma^R_{e^+e^-}\mathcal{B}_\mathcal{R}(\phi\ \eta')\Gamma^R_{tot}}}{s - M_R^2 + iM_R\Gamma^R_{tot}}\cdot\sqrt{\frac{\Phi(s)}{\Phi(M_R)}} \quad (4)$$

$$\Phi(\sqrt{s}) = \frac{\sqrt{[s-(m_{\eta'}+m_\phi)^2][s-(m_{\eta'}-m_\phi)^2]}}{2\cdot s} \quad (5)$$

$$\Phi(M) = \frac{\sqrt{[M_R^2-(m_{\eta'}+m_\phi)^2][M_R^2-(m_{\eta'}-m_\phi)^2]}}{2\cdot M_R^2} \quad (6)$$

where M_R is the mass of the resonance, Γ^R_{tot} the total width, $\Gamma^R_{e^+e^-}$ the e^+e^- partial width, $\mathcal{B}_\mathcal{R}(\phi\ \eta')$ the branch fraction of the resonance decay to $\phi\ \eta'$, φ the phase angle between the resonance and the phase-space contribution, $\Phi(\sqrt{s})$ the phase space factor for and S-wave two-boday system. $m_{\eta'}$ and m_ϕ is the mass of η' and ϕ, respectively.

The fit has two solutions with equally good fit quality, $\chi^2/ndf = 27.73/15$, and identical masses, widths of the resonances and the product of the electronic widths with the branching fractions, while the phases are different. The mass and width of the resonance are determined to be $M = (2182.4 \pm 5.1)$ MeV$/c^2$and $\Gamma = (142.2 \pm 16.6)$ MeV, where the error is statistical only. Figure 3 shows the fit result and the parameters of the resonance are summarized in Table IV. The resonance has a mass consistent with that of $\phi(2170)$ within 1.0 σ. However, its measured width is much larger than the average width, 83±12 MeV, of the $\phi(2170)$. The significance of the resonance is determined to be 12.47σ (including systematic uncertainties) by comparing the change of $\Delta(\chi^2)$ with and without the R amplitude in the fit and taking the change of number of degree of freedom $\Delta n.d.f = 4$ into account.

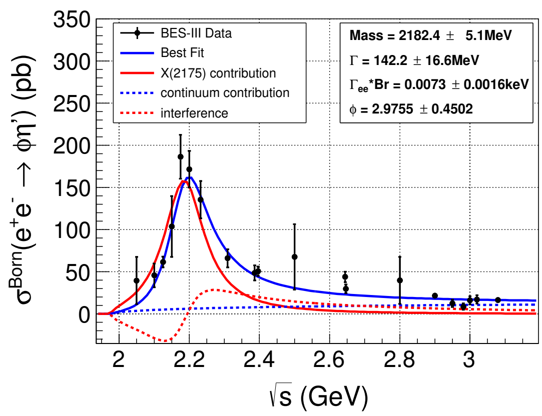

FIG. 3: The fit of cross section line shape of $e^+e^- \to \phi\ \eta'$ is obtained by the Probability Density Function 3 in this work.

TABLE IV: Results of the fit to the $e^+e^- \to \phi\eta'$ cross section. The error is statistical only.

Parameters	Solution I	Solution II
M_R (MeV/c^2)	2182.4 $\pm$ 5.1	
Γ^R_{tot} (MeV)	142.2 $\pm$ 16.6	
$\mathcal{B}_\mathcal{R}\Gamma^R_{e^+e^-}$(keV)	0.0073$\pm$ 0.0016	
φ(rad)	2.9755 $\pm$ 0.4502	-0.1662 $\pm$ 0.4473

A. Systematic Uncertainty for resonance parameters

The systematic uncertainties of the resonant parameters in the fit to the energy-dependent cross section of $e^+e^- \to \phi\eta'$ are mainly from the uncertainties of c.m. energy determination, energy spread, the cross section measurement and the parametrization of the BW function.

- *Energy scale*: The uncertainty from the c.m. energy measurement is studied by taking the uncertainty of the c.m. energy 1.6 MeV at 2.125 GeV [34] into consideration. This common uncertainty will propagate only to the masses of the resonance with the same amount, i.e.,$\pm$ 1.6 MeVc^2.

- *Energy spread*:

  To estimate the uncertainty from the energy spread, the PDF convoluted with a Gaussian function with a resolution of 1.6 MeV [35] is used to fit the data, and the uncertainty is estimated by comparing the results with the nominal ones.

VIII. SUMMARY AND DISCUSSION

In summary, based on data samples collected with the BESIII detector at the BEPCII collider at 20 c.m. energies from 2.050 to 3.080 GeV, we perform a precise cross section measurement of $e^+e^- \to \phi\ \eta'$. By assuming the $\phi\ \eta'$ come from a single resonance, we extract the mass and width of the resonance to be 2180.3 ± 4.9 MeV and 140.1 ± 16.4 MeV,respectively. Here, the first errors are statistical and the second ones are systematic. Its statistical significance is estimated to be large than 12.0 σ.

Considering the conservation laws, J^{PC} of the resonance is equal to be 1^{--}. Due to its mass comparable to the $\phi(2170)$, the resonance agrees with the $\phi(2170)$ resonance reported by previous experiments. However, our measured width is much larger than the $\phi(2170)$ average width reported by previous experiments. If we assume it is the same resonance as the $\phi(2170)$, a new decay channel of $\phi(2170) \to \phi\eta'$ has been observed first time.

IX. ACKNOWLEDGMENTS

The BESIII collaboration thanks the staff of BEPCII and the IHEP computing center and the supercomputing center of USTC for their strong support. This work is supported in part by National Key Basic Research Program of China under Contract No. 2015CB856700; National Natural Science Foundation of China (NSFC) under Contracts Nos. 11625523, 11635010, 11735014, 11335008, 11375170, 11475164, 11475169, 11605196, 11605198, 11705192; National Natural Science Foundation of China (NSFC) under Contract No. 11835012; the Chinese Academy of Sciences (CAS) Large-Scale Scientific Facility Program; Joint Large-Scale Scientific Facility Funds of the NSFC and CAS under Contracts Nos. U1532257, U1532258, U1732263, U1832207, U1532102, U1732263, U1832103; CAS Key Research Program of Frontier Sciences under Contracts Nos. QYZDJ-SSW-SLH003, QYZDJ-SSW-SLH040; 100 Talents Program of CAS; INPAC and Shanghai Key Laboratory for Particle Physics and Cosmology; German Research Foundation DFG under Contract No. Collaborative Research Center CRC 1044; Istituto Nazionale di Fisica Nucleare, Italy; Koninklijke Nederlandse Akademie van Wetenschappen (KNAW) under Contract No. 530-4CDP03; Ministry of Development of Turkey under Contract No. DPT2006K-120470; National Science and Technology fund; The Knut and Alice Wallenberg Foundation (Sweden) under Contract No. 2016.0157; The Swedish Research Council; U. S. Department of Energy under Contracts Nos. DE-FG02-05ER41374, DE-SC-0010118, DE-SC-0012069; University of Groningen (RuG) and the Helmholtzzentrum fuer Schwerionenforschung GmbH (GSI), Darmstadt

[1] B. Aubert *et al.* (BABAR Collaboration), Phys. Rev. D **74**, 091103(R) (2006); **76**, 012008 (2007).
[2] C. P. Shen *et al.* (BELLE Collaboration), Phys. Rev. D **80**, 031101(R) (2009).
[3] M. Ablikim *et al.* (BES Collaboration), Phys. Rev. Lett. **100**, 102003 (2008).
[4] M. Ablikim *et al.* (BESIII Collaboration), Phys. Rev. D **91**, 052017 (2015).
[5] M. Ablikim *et al.* (BESIII Collaboration), Phys. Rev. D **99**, 012014 (2019).
[6] M. Ablikim *et al.* (BESIII Collaboration), Phys. Rev. D **99**, 032001 (2019).
[7] Gui-Jun Ding and Mu-lin Yan, Phys. Lett. B. **650**, 390 (2007).
[8] P. R. Page, E. S. Swanson, A. P. Szczepaniak, Phys. Rev. D **59** 034016 (1999).

[9] Gui-Jun Ding and Mu-lin Yan, Phys. Lett. B. **657**, 49 (2007).

[10] T. Barnes, N. Black, P. R. Page, Phys. Rev. D **68** 054014 (2003).

[11] Zhi-Gang Wang, Nucl. Phys. **A791**, 106 (2007).

[12] Hua-Xing Chen, Xiang Liu, Atsushi Hosaka, and Shi-Lin Zhu, Phys. Rev. D. **78**, 034012 (2008).

[13] E. Klempt and A. Zaitsev, Phys. Rep. **454**, 1 (2007).

[14] Y. B. Dong *et al.,* Phys. Rev. D. **96**, 074027 (2017).

[15] S. L. Zhu, Int. J. Mod. Phys. E **17**, 283 (2008).

[16] A. M. Torres, K. P. Khemchandani, L. S. Geng, M. Napsuciale, and E. Oset, Phys. Rev. D **78**, 074031 (2008).

[17] M. Ablikim *et al.* (BESIII Collaboration), arXiv:1901.00085.

[18] B. Aubert *et al.,* (BABAR Collaboration), Phys. Rev. D **77**, 092002 (2008).

[19] B. Aubert *et al.,* Phys. Rev. D. **76**, 092005 (2007).

[20] M. Ablikim *et al.* (BESIII Collaboration), Nucl. Instrum. Meth. A **614**, 345 (2010).

[21] C. H. Yu *et al.,* Proceedings of IPAC2016, Busan, Korea, 2016, doi:10.18429/JACoWIPAC2016-TUYA01.

[22] S. Agostinelli *et al.* (GEANT4 Collaboration), Nucl. Instrum. Methods Phys. Res., Sect. A **506**, 250 (2003).

[23] R. G. Ping, Chin. Phys. C **38**, 083001 (2014).

[24] D. J. Lange, Nucl. Instrum. Methodes Phys. Res., Sect. A **462**, 152 (2001).

[25] R. G. Ping, Chin. Phys. C **32**, 599 (2008).

[26] M. Tanabashi *et al.* (Particle Data Group), Phys. Rev. D **98**, 030001 (2018).

[27] B. Andersson and H. Hu, arXiv:hep-ph/9910285.

[28] E. A. Kuraev and V. S. Fadin, Yad. Fiz. **41**, 733 (1985).

[29] S. Actis et al. Eur. Phys. J. C **66**, 585 (2010).

[30] M. Ablikim *et al.* (BESIII Collaboration), Chin. Phys. C **41**, 063001 (2017).

[31] M. Ablikim *et al.* (BESIII Collaboration), Phys. Rev. D. **99**, 011101 (2019).

[32] M. Ablikim *et al.* (BESIII Collaboration), Phys. Rev. D. **87**, 012002 (2013).

[33] M. Ablikim *et al.* (BESIII Collaboration), Phys. Rev. L. **118**, 092001 (2017).

[34] M. Ablikim *et al.,* Chin. Phys. C **41**, 113001 (2017).

[35] E. V. Abakumova *et al.* Nucl. Methods Phys. Res. , Sect. 659, 21 (2011).